Research Article

Assessment of absorbed dose in deformed breast tissue by Monte Carlo simulation

Mansour Ashoor[1] · Abdollah Khorshidi[2,3]

Abstract

The main concern in radiotherapy of the breast is covering the target volume and increasing the dose absorbed by tumor cells. The aim is intended to provide a pertinent moldable perspective to the currently utilized methods of calculating Kerma value (KV) as a function of distance from nipple. The KV in the breast deformed for two shapes, such as cylindrical–conical (CC) and cubic–rectangular (CR), was simulated using Monte Carlo method with appropriate assumptions and a 2 MeV X-ray system. The source was positioned near the right breast. Simulation results demonstrated that decreasing height of CR shape reduced the absorption and scattering cross-sections as well as the KV. Relative accumulated dose for a CR-shaped breast was 96.89% lower than that for CC-shaped breast. The KV in the breast decreased with increasing distance from the nipple (depth) for both shapes, but for right and left breasts in CR form was independent from depth with no change between breasts as depth increased. The relative difference in KV between the breasts was significant for CR shape, in which the KV was high at low depths and decreased linearly with increasing depth. Tumors are often differentiable in the breast form; hence, the normal breast should be deformed into CR shape to improve the degree of tissue protection in adjuvant radiotherapy. It is expected that the dose absorbed by the gland will be more strongly increased for CC shape rather than for CR shape in radiation therapy.

Keywords Deformed breast · Kerma value · Cylindrical–conical · Cubic–rectangular · MCNPX code · Radiotherapy

Abbreviations

KV	Kerma value
CC	Cylindrical–conical
CR	Cubic–rectangular
MCNPX	Monte Carlo N-particles code version X
RB and LB	Right and left breasts

1 Introduction

According to the World Health Organization, approximately one million people worldwide are diagnosed with breast cancer annually. Predominately a disease of high-income developed countries, breast cancer accounts for 22% of all cancers in women worldwide [1]. The most common diseases in breast cancer in women are calcification, ductal, tubular, and lobular carcinoma formations [2, 3], which are regularly distinguished by mammography images. If the cancer is detected in the early stages of growth, it may be treated quickly [4–7]. The dose absorbed by an individual patient after an exposure to ionizing radiation is seldom documented as a routine matter by imaging. In addition, no standardized clinical protocols exist to quantify the dose to the breast tissue of the individual, and the absorbed doses vary widely among individual patients. Therefore, it is not possible to evaluate accurately the dose of radiation absorbed by the breast for a population from imaging. The X-ray radiation is the standard

✉ Abdollah Khorshidi, abkhorshidi@yahoo.com; Mansour Ashoor, ashoor_44@yahoo.com | [1]Radiation Application Research School, Nuclear Science and Technology Research Institute, P.O. Box 113653486, Tehran, Iran. [2]School of Paramedical, Gerash University of Medical Sciences, P.O. Box 7441758666, Gerash, Iran. [3]Medical Radiation Engineering Department, Islamic Azad University, Parand Branch, P.O. Box 3761396361, Parand, Iran.

method in radiation therapy, but the risk of damage to the normal tissues exists. The mean glandular dose is used as a quantity for determining the radiation risk in the course of radiation treatment. The absorbed dose is estimated with the assumption of homogeneous tissue distribution. In reality, the accuracy of the estimate is controversial, because the breast is composed of inhomogeneous tissues [8–10]. This study is intended to provide a pertinent moldable perspective to the currently utilized methods of calculating the KV as a function of distance from nipple. In this study, a 2 MeV X-ray system is simulated by the Monte Carlo method with various shapes of breast deformation, with the aim of diminishing the transfer of doses to adjacent healthy tissues.

2 Methods and materials

2.1 Theory

The interactions of radiation with matter are diverse because of the media diversity of energy and material. In this study, the Kerma parameter was evaluated in a tissue-equivalent material by Monte Carlo simulations of a simplified model of the compressed or deformed breast. To decrease the Kerma value (KV) and to increase the signal-to-noise ratio, methods based on both the shielding design and the deformation of the breast may be used. Here, two shapes of deformed breast tissue, known as cylindrical–conical (CC) and cubic–rectangular (CR), are introduced and compared, as shown in Fig. 1. Both shapes have the same breast volume, since the breast density remains unchanged under deformation. With this assumption, the relationship between the two geometric shapes may be expressed as follows:
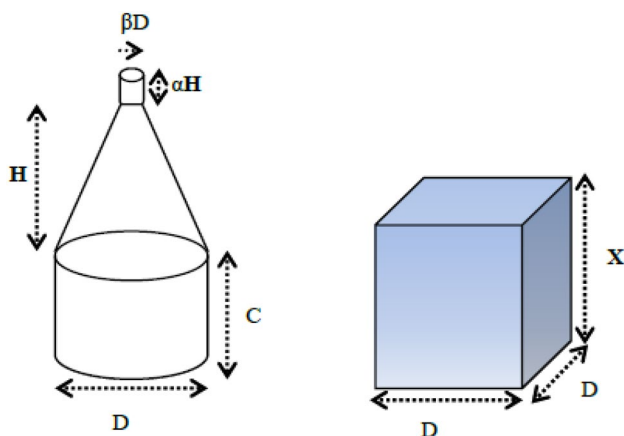

Fig. 1 Schematic of the deformed breast in simulation as cylindrical–conical shape (left), and cubic–rectangular shape (right)

$$X = \pi \times \left(\frac{(1 + 3\alpha\beta^2)H}{12} + \frac{C}{4} \right) \tag{1}$$

$$C + (1 + \alpha)H = \text{constant}\,(K) \tag{2}$$

where α and β are trivial fractional dimensions of the cone height (H) and cylinder diameter (D), respectively. K is the total height of the CC shape. X is the height of the CR shape, indicating a model for the deformed breast. The most important indices of Eqs. (1, 2) are independent from the value of D, with respect to the aforementioned assumptions. In other words, the base area of the breast is independent of the computations and results. These equations are represented schematically in Fig. 2 with K amounts of 10, 15, and 20 cm and α and β values approaching zero. In this special case, the rate of decrease in X with the increase in H is theoretically determined to have the slope of − 0.5235, indicating a 152.5° angle, referred to henceforth as the deformed angle of the breast, in which there is optional changing rate on the breast. The rate of change in X versus H is always a constant value under all circumstances by definition.

2.2 Simulation method and computation of geometrical parameters

To protect neighboring tissue, the radiation is blocked with shielding. The complex transportations and interactions of particles were modeled with the Monte Carlo method and MCNP code [11]. Here, the Monte Carlo N-Particles code version X (MCNPX) was used, which obtains a history of the contribution of each photon in producing the KV and dose rate. This code is applicable for the accessibility and control offered overall parameters included in the computations. The code permits the tractable detection of the particles based on the cross-sections of different interactions, as well as providing the flux, dose, and Kerma determination. These output factors in the form of tallies, which indicate the amount of energies deposited in the tissues, have been characterized by this code in different situations. An estimation of the energy per gram output was performed using the F6 tally, in which the energies accumulated in the defined geometric cells, yielding energy released in a mass unit, and the KV were calculated as follows:

$$F6 = \rho_a/\rho_g \iiint H(E)\Phi\,(E, t)\,dE\,dV\,dt \tag{3}$$

where $\Phi(E)$, E, t, V, ρ_a, ρ_g, and H(E) are the energy-dependent fluence (particles/cm^2 MeV), energy value, time, volume, atomic density, mass density, and heating response function, respectively. The KV, corresponding to F6, increases with increasing X-ray energy, absorption
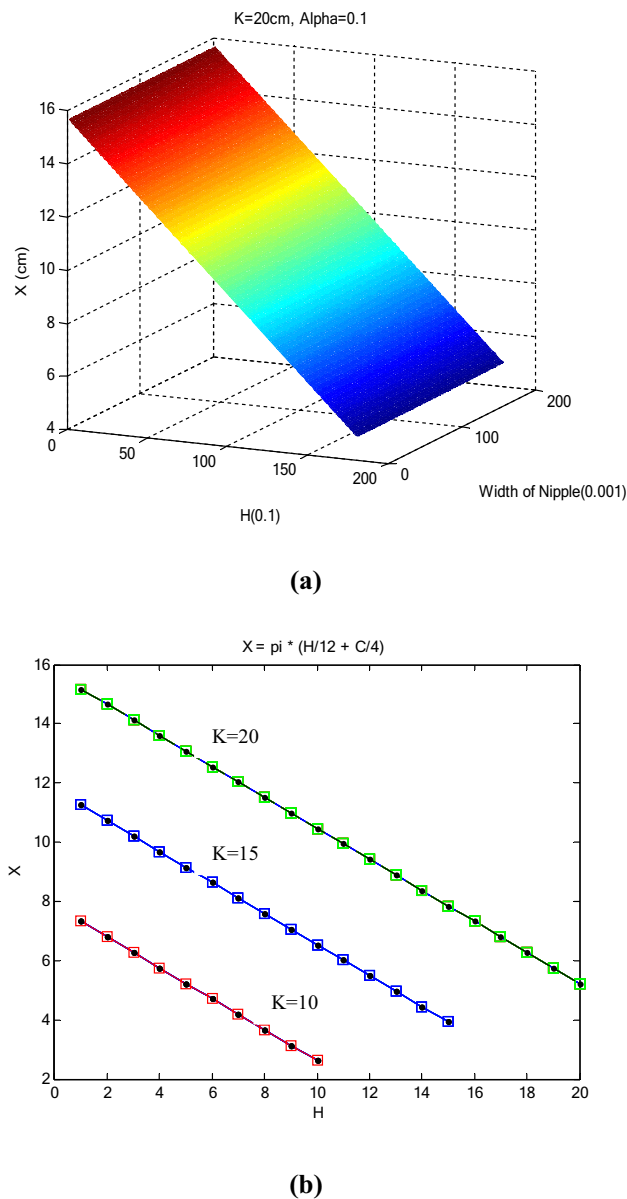
(a)

(b)

Fig. 2 a The height of the cube (X) as a function of that of the cone (H) and the width of the nipple at $\alpha = 0.1$ and K = 20 cm. **b** The height of the cube (X) as a function of that of the cone (H) while the summation of the cone heights is constant (measured in cm) for K amounts of 10, 15, and 20 cm at $\alpha = \beta = 0$

$$FMn = C \int \Phi(E) R_m(E) \, dE \qquad (4)$$

where R(E) is an operator of the additive and/or multiplicative response functions from the MCNPX cross-section libraries or other specifically designated quantities. The constant *C* is an arbitrary scalar quantity used for normalization. The material number *m* must appear on an *Mm card*. The F4 and/or F2 tallies used in MCNP are track length tallies, which sum the distances traveled by particular types of particles in defined volumes and/or surfaces. The units of volume- and/or surface- and time-normalized F4 and/or F2 tallies are particle/cm^2. Investigation of the energy transfer occurred by determining the characteristics of the cross-section of an interaction, as the absorption and scattering cross-sections of the simulations were considered from the ENDF/B-VII.1 libraries [12]. To suitably model the breast, the real size, shape, thickness, width, length, and surface area were considered. The breast volume ranges between 400 and 1200 cm^3, so the volume of 942.5 cm^3 was used for these simulations [13]. The input data included a combination of defined cells and surfaces in which variously shaped breasts were located in a finite air sphere at first. Then, density of various tissues in the deformed breast was considered in a three-dimensional scheme. The X-ray energy was 2 MeV, a source that propagates towards the breast to assess the dose and Kerma values using relevant tally cards.

3 Results

The changes in CR height versus the changes in cone height of the CC shape and the size variations of the breast nipple at the total height of 20 cm and $\beta = 0.1$ is shown in Fig. 2a. As the cone height increases, the CR height decreases at a distinct slope; the minimum deformation occurs when the conic part of the CC shape is insignificant compared to the cylindrical component. Thus, the largest breast has the lowest height in the CC shape, and will absorb the highest dose compared to the average situation. Figure 2b indicates that, as the total CC height changes, the changes in CR height versus the changes in CC height occur with a constant slope under the assumption of negligible nipple size; this slope is defined as the deformed angle. This angle varies negligibly with the changing size of the nipple; thus, when the tumor was positioned in the nipple itself, the deviations in the computations were trivial.

The geometric results of the output files from the MCNPX code for the CC, CR, and CC–CR shapes have been shown in Fig. 3a–c respectively. The tissue density and dimensions of the CR shape were 1.04 g/cm^3 and 12

coefficient, and particle flux. The deformation of the geometric shape of the defined breast changes the cross-sectional area of the breast, which decreases the KV and dose rate. The F4 and/or F2 tallies, along with the *FMn card*, in which the particle flux in a defined cell and/or surface (estimated volumetrically or by area) may also be used by this code as follows:
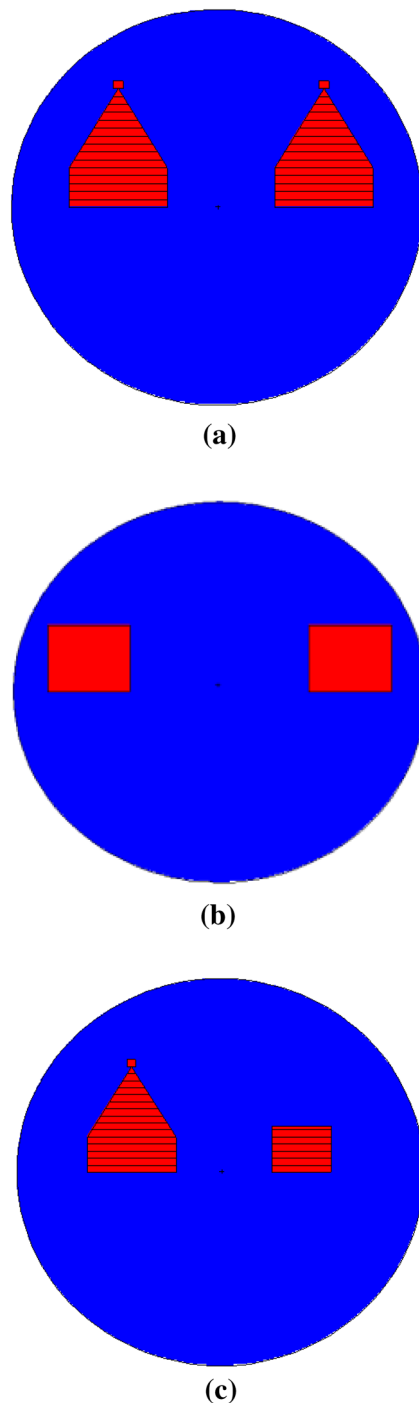
(a)

(b)

(c)

Fig. 3 **a** The simulated CC shape of the breast. **b** The simulated CR shape of the deformed breast. **c** The simulated CC and CR shapes of the breasts

cm × 12 cm × 6.55 cm, respectively. The CC shape was a cylinder with H = 1 and D = 1.2 cm, a cone with H = 10 and D = 12 cm, and a cylinder with H = 5 and D = 12 cm. The number of particles for the simulation was 10^7. The mean error of the simulations in the output was 2%.

The distributions of the simulated dose and KVs for the CC shape according to depth were similar, correspondingly for tissue and air equivalents used in the code. With local increases in depth, both quantities are decreased because of the decrease in the number of incident particles, as shown in Fig. 4a. A relative difference is observed between the dose and KV for the CC shape according to depth, because of statistical fluctuations in the computations of the code, as shown in Fig. 4b. At low values of depth, this difference is very trivia; and as the depth increases, the difference is increased because the secondary interactions and scattering factors are increased.

For the CC shape, the distribution of KV in both right and left breasts (RB and LB) with the source near the RB indicated that the KV for the RB exceeds that of the LB, because the amount of attenuation is increased with increasing depth and distance from the source, as shown in Fig. 4c. The relative difference between KVs for the RB and LB of CC shape as a function of depth has been shown in Fig. 4d. This difference is high at low values of depth, and with increasing depth, the difference decreases as an exponential function with a slope of 0.022 MeV/g cm and approaches zero at depths of > 18 cm.

For the CR-shaped deformed breast, the distribution of KV in both LB and RB with a source near the RB indicated that the KV is independent of the depth, which differs from the case with the CC shape. The differences between LB and RB with increasing depth are insignificant, as indicated in Fig. 5a. The relative difference between the KVs in the RB and LB for the CR shape as a function of the depth is shown in Fig. 5b. This difference is, again, high at low values of depth, but decreases with increasing depth as a linear function with a slope of 0.005 MeV/g cm.

In addition, the distribution of KV in the LB for the CR shape and in the RB for the CC shape as a function of depth has been illustrated in Fig. 6a. The changes in KV between breasts are independent of the depth in the CR shape, and the difference between KV in the LB and RB with increasing depth is insignificant. However, for the CC shape, the change in KV at low values of depth gradually decreases with increasing depth; at high values of depth, degree of difference in KV severely decreased because of the beam-hardening phenomenon. The relative differences between the LB for CR shape and the RB for the CC shape are indicated in Fig. 6b to be very high at low depth, and with increasing depth decreases as a linear function with a slope of 0.013 MeV/g cm.

Table 1 shows the accumulated KVs in the LB and RB for the CR and CC shapes, correspondingly. The relative accumulated KV in the CC shape is 96.89% more than that in the CR shape. This indicates that the normal breast should be positioned in the CR shape in treatment, because the
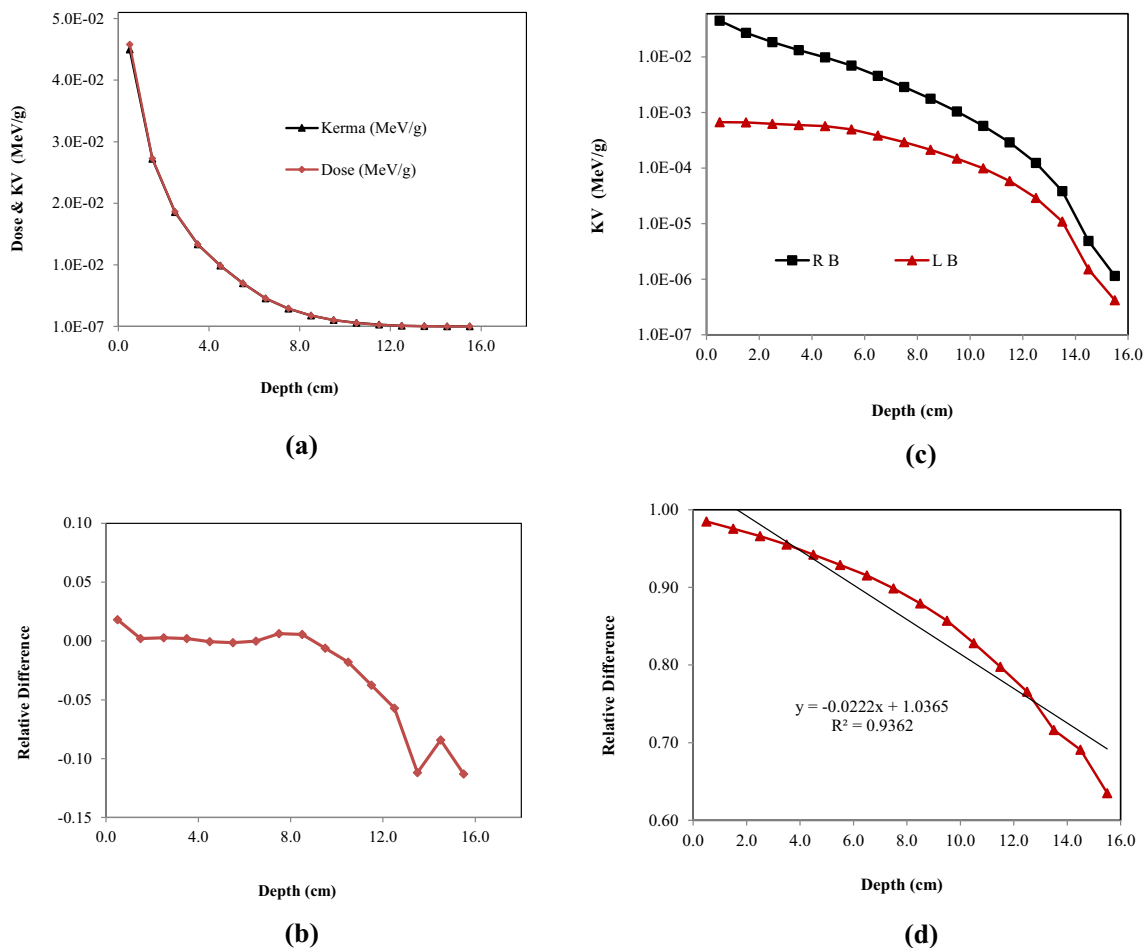
(a)

(b)

(c)

(d)

Fig. 4 **a** The simulated dose rate and KV as a function of depth for the CC shape. **b** The relative difference between the dose rate and KV for the CC shape at 2 MeV irradiation. **c** The simulated KV in the RB and LB for the CC shape. **d** The relative difference in the KV in the LB and RB for the CC shape

probability of forming tumors in the nipple of the breast is high.

4 Discussion

The purpose of irradiating tissues is the recognition of abnormalities and the treatment of abnormal tissues with a minimum dose delivered to the other healthy tissues. This may be achieved using suitable shielding, correct deformation of the normal tissues, or both [13–22]. Here, the deformation from the CC to CR shape was simulated by the Monte Carlo method and the dose and KVs were compared between shapes. Since the pair-production cross section is higher than the photoelectric at 2 MeV energy, the pair production was taken into account.

The Monte Carlo simulation can be analyzed by the interactions of rays in the materials, based on the scattering and absorption cross-sections arising from the

photoelectric and Compton processes, by which the flux, dose, and KV can be calculated. The photoelectric coefficient decreases with the increase of the energy at low energies, and is insignificant at the simulated energy of 2 MeV. By contrast, the Compton coefficient is decreased with increasing energy at low energies, but after a critical energy value is reached, the coefficient becomes constant with the increase of energy before severely decreasing above a second critical value. The Compton coefficient is constant at energies of approximately 2 MeV. The contribution of the Compton and photoelectric coefficients at the energy studied were 98% and 2%, respectively via the simulations. In general, at this energy value, the Compton process dominates rather that the photoelectric process; this indicates that the number of scattered photons is increased and the dose absorbed by other organs is consequently increased. The simulated KV at 2 MeV for the CC shape decreased locally with increasing depth in the breast, because of the decreased energy of the rays. The
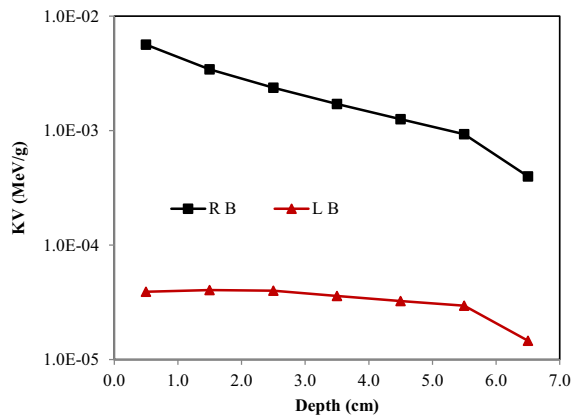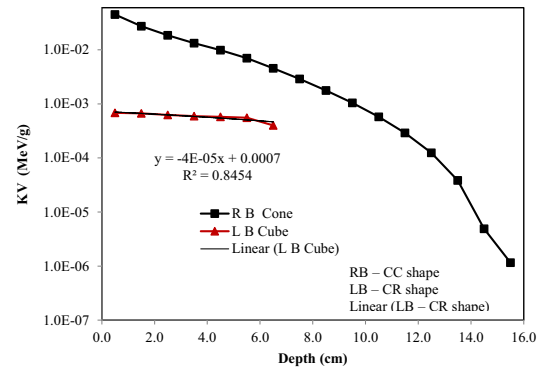
(a)
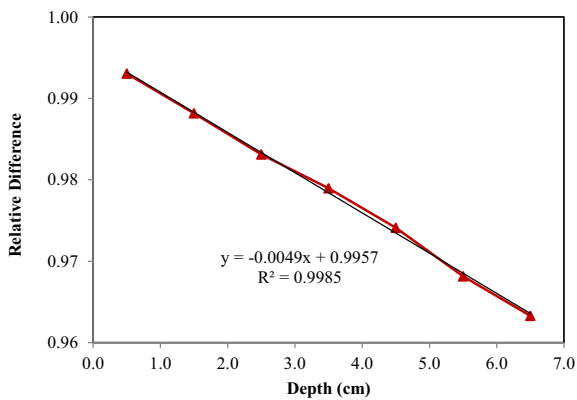
(b)

Fig. 5 **a** The simulated KV as a function of depth for the CR shape. **b** The relative difference in the KV in the LB and RB for the CR shape

(a)   The simulated KV in the LB for the CR shape and in the RB for the CC shape

(b)   The relative difference in KV between the LB for CR shape and the RB for the CC shape

Fig. 6 **a** The simulated KV in the LB for the CR shape and in the RB for the CC shape. **b** The relative difference of KV between the LB for CR shape and the RB for the CC shape
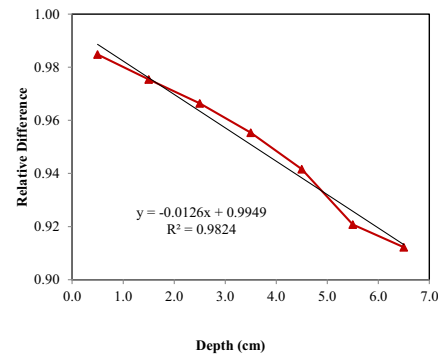
KV at different depths was approximately constant for the CR shape; the probability of interactions increased for the CC shape due to the large solid angle of the geometry. Smaller solid angles correspond to lower probabilities of interactions; the KV decreases with decreased solid angle, because the production and interaction of the rays with the material follow random models.

The accuracy in the dose computations is very important; the total error should be lower than 5%. As abnormal tissues are irradiated, neighbouring healthy tissues absorb some of the dose from the scattered rays by necessity [23]. The non-target tissues in the breast receive an average of 14.3% of the dose [24–26]. There is a minor difference between the calculated and reported values, resulting from fluctuations and statistical oversights [27]. However, the difference in values is neglected in practical applications [28].

The deformed angle calculated from Eq. (1) is a constant criterion under all situations. A minor error will exist in the results when the protocol proposed here is followed,

Table 1 The accumulated KV in the LB for the CR shape and in the RB for the CC shape

	Accumulated Kerma (MeV/g)	Cube (deformed LB)	Relative difference
Accumulated Kerma (MeV/g)	1.322×10^{-1}	4.099×10^{-3}	96.89%

because the breast cannot precisely take the CR shape because of the curvature of the borders of the volume.

5 Conclusions

A new method was proposed to decrease the dose absorbed in adjacent healthy tissues based on the deformation of breast tissue. This deformation of the breasts into the CR shape was permitted by the flexibility of the breast tissue. The absorbed dose and KVs were simulated

in the different shapes by the MCNPX code. The results showed that at low energy of ray, the dose and Kerma values were similar, and with increasing depth, both decreased. The Kerma at different depths was approximately constant for the CR shape, but decreased linearly in the CC shape. The probability of ray-material interactions increased for the CC shape due to the large solid angle of the geometry. Smaller solid angles correlate to lower probabilities of interactions, which will decrease the Kerma because the production and interaction of rays follow random models. Finally, deformation of the breast may prevent injuries to healthy tissue in the treatment and imaging processes.

Compliance with ethical standards

Conflict of interest The authors have declared no conflict of interest.

Human participants and/or animals No participation: "This article does not contain any studies with human participants or animals performed by any of the authors."

References

1. Ferlay J, Colombet M, Soerjomataram I, Mathers C, Parkin DM, Pineros M, Znaor A, Bray F (2019) Estimating the global cancer incidence and mortality in 2018: GLOBOCAN sources and methods. Cancer Epidemiol 144(8):1941–1953. https://doi.org/10.1002/ijc.31937
2. Taherian-Esfahani Z, Taheri M, Dashti S, Kholghi-Oskooei V, Geranpayeh L, Ghafouri-Fard S (2019) Assessment of the expression pattern of mTOR-associated lncRNAs and their genomic variants in the patients with breast cancer. J Cell Physiol. https://doi.org/10.1002/jcp.28767
3. Maajani K, Khodadost M, Fattahi A, Pirouzi A (2019) Survival rates of patients with breast cancer in the Eastern Mediterranean Region: a systematic review and meta-analysis. East Mediterr Health J. https://doi.org/10.26719/emhj.19.091
4. Ashoor M, Khorshidi A (2019) Evaluation of crystals' morphology on detection efficiency using modern classification criterion and Monte Carlo method in nuclear medicine. Proc Natl Acad Sci India Sect A Phys Sci 89:579–585. https://doi.org/10.1007/s40010-018-0482-x
5. Ashoor M, Khorshidi A, Sarkhosh L (2019) Estimation of microvascular capillary physical parameters using MRI assuming a pseudo liquid drop as model of fluid exchange on the cellular level. Rep Pract Oncol Radiother 24(1):3–11. https://doi.org/10.1016/j.rpor.2018.09.007
6. Soltani-Nabipour J, Khorshidi A, Noorian B (2020) Lung tumor segmentation using improved region growing algorithm. Nucl Eng Technol. https://doi.org/10.1016/j.net.2020.03.011
7. Khorshidi A (2020) Assessment of SPECT images using UHRFB and other low-energy collimators in brain study by Hoffman phantom and manufactured defects. Eur Phys J Plus 135:261. https://doi.org/10.1140/epjp/s13360-020-00238-6
8. Papie M, Faghihi R, Sina S, Sarshogh S (2019) The effect of breast phantom material on the dose distribution in AccuBoost brachytherapy. Iran J Med Phys 16(1):91–97. https://doi.org/10.22038/ijmp.2018.28204.1303
9. Khorshidi A, Abdollahi A, Pirouzi A, Hosseini SH (2020) Band pass filter plan in fluoroscopy for high energy range. SN Appl Sci 2:90. https://doi.org/10.1007/s42452-019-1885-2
10. Sinousy DM, Attalla EM, Hanafy MS, Abouelenein HS, Abdelmajeed M, Osama M (2019) Dosimetric study of tissue heterogeneity correction for breast conformal radiotherapy. Iran J Med Phys 16(2):179–188. https://doi.org/10.22038/ijmp.2018.31579.1374
11. Hughes HG et al (2002) MCNPX™ 2.4.0, user's manual—version 2.4.0, LA-CP-02-408. Los Alamos National Laboratory, Los Alamos
12. ENDF/B-VII.1 (2011) US Evaluated Nuclear Data Library. https://www-nds.iaea.org/exfor/endf.htm. Accessed 2 Sept 2015
13. Kayar R, Civelek S, Cobanoglu M, Gungor O, Catal H, Emiroglu M (2011) Five methods of breast volume measurement: a comparative study of measurements of specimen volume in 30 mastectomy cases. Breast Cancer 5:43–52. https://doi.org/10.4137/BCBCR.S6128
14. Khorshidi A (2016) Gold nanoparticles production using reactor and cyclotron based methods in assessment of 196,198Au production yields by 197Au neutron absorption for therapeutic purposes. Mater Sci Eng C 68(1):449–454. https://doi.org/10.1016/j.msec.2016.06.018
15. Ashoor M, Khorshidi A, Sarkhosh L (2019) Introducing a novel coefficient on mixed-nanoparticles material: relationship between the theoretical and experimental densities. Heliyon 5(7):e02056. https://doi.org/10.1016/j.heliyon.2019.e02056
16. Khorshidi A (2019) Radiochemical parameters of molybdenum-99 transmutation in cyclotron-based production method using a neutron activator design for nuclear-medicine aims. Eur Phys J Plus 134:249. https://doi.org/10.1140/epjp/i2019-12568-3
17. Ashoor M, Khorshidi A, Sarkhosh L (2020) Appraisal of new density coefficient on integrated-nanoparticles concrete in nuclear protection. Kerntechnik 85(1):9–14. https://doi.org/10.3139/124.190016
18. Khaleghi G, Soltani-Nabipour J, Khorshidi A, Taheri F (2019) Design of band-pass filters by experimental and simulation methods at the range of 100–125 keV of X-ray in fluoroscopy. Int J Biomed Technol. https://doi.org/10.1504/ijbet.2019.10025733
19. Ahmadi M, Soltani-Nabipour J, Khorshidi A, Negarestani A, Taheri F (2020) Electrical duality design for the radon-222 decay chain. Microelectron Reliab 107:113620. https://doi.org/10.1016/j.microrel.2020.113620
20. Banihashemi N, Soltani-Nabipour J, Khorshidi A, Mohammadi H (2020) Quality control assessment of Philips digital radiography and comparison with Spellman and Samsung systems in Tehran Oil Ministry Hospital. Eur Phys J Plus 135:269. https://doi.org/10.1140/epjp/s13360-020-00275-1
21. Nabipour JS, Khorshidi A (2018) Spectroscopy and optimizing semiconductor detector data under X and γ photons using image processing technique. J Med Imaging Radiat Sci 49(2):194–200. https://doi.org/10.1016/j.jmir.2018.01.004
22. Asgari A, Ashoor M, Sarkhosh L, Khorshidi A, Shokrani P (2019) Determination of gamma Camera's calibration factors for quantitation of diagnostic radionuclides in simultaneous scattering and attenuation correction. Curr Radiopharm 12(1):29–39. https://doi.org/10.2174/1874471011666180914095222
23. Soltani-Nabipour J, Khorshidi A, Shojai F, Khorami K (2020) Evaluation of dose distribution from 12C ion in radiation therapy by FLUKA code. Nucl Eng Technol. https://doi.org/10.1016/j.net.2020.03.010

24. Aaltonen P, Brahme A, Lax I, Levernes S, Näslund I, Reitan JB, Turesson I (1997) Specification of dose delivery in radiation therapy: recommendation by the Nordic Association of Clinical Physics (NACP). Acta Oncol 10:1–32

25. Bhatnagar AK, Brandner E, Sonnik D, Wu A, Kalnicki S, Deutsch M, Heron DE (2006) Intensity modulated radiation therapy (IMRT) reduces the dose to the contralateral breast when compared to conventional tangential fields for primary breast irradiation. Breast Cancer Res Treat 96(1):41–46. https://doi.org/10.1007/s10549-005-9032-8

26. Khorshidi A, Rajaee A, Ahmadinejad M, Ghoranneviss M, Ettelae M (2014) Low energy electron generator design and depth dose prediction for micro-superficies tumors treatment purposes. Phys Scr 89:095001. https://doi.org/10.1088/0031-8949/89/9/095001

27. Khan MF (2009) The physics of radiation therapy. Williams and Wilkins A Waverly Company, London

28. Commissioning and Quality Assurance of Computerized Planning Systems for Radiation Treatment of Cancer (2004) IAEA technical report series 430

Publisher's Note Springer Nature remains neutral with regard to jurisdictional claims in published maps and institutional affiliations.